Optimal Disturbance Rejection by LTI Feedback Control in a Laser Beam Steering System

Pawel K. Orzechowski, James S. Gibson, Tsu-Chin Tsao

***Abstract*—This paper presents an optimal control design and experimental implementation for pointing and disturbance rejection in a laser beam steering system. To compensate for broadband disturbances due to atmospheric turbulence in the optical path and mechanical vibration of the laser and optical components, the linear quadratic Gaussian (LQG) controller includes a stochastic disturbance model, as well as integral action for tracking low-frequency disturbances and commands.**

The experimental system consists of a two-axis tilt mirror actuated by piezo-electric actuators, a second actuated tilt mirror to generate disturbances, a position sensing device that senses the location of the beam on a target plane, and a real-time computer for digital control. System identification is used to determine a state-space model of the beam steering system for use in control system design. Experimental results are presented to demonstrate the effectiveness of the LQG optimal disturbance rejection in desired bandwidths.

I. Introduction

Laser beam steering or pointing refers to active control of the beam direction to stabilize the beam image at a desired location. Commercial, scientific, and military applications include optical communication systems and adaptive optics for astronomy and high-energy laser systems, and surveillance [1–3]. For example, if a surveillance camera's alignment is controlled by beam steering mirrors, obtaining still images or tracking a fast-moving target requires high-performance feedback of the beam steering mirrors. In such applications, errors resulting from poorly controlled beam steering will directly affect the camera line of sight and produce unwanted jitter. In the context of adaptive optics, where the distorted wavefront is compensated by a deformable mirror, the beam track loop represents the first-order spatial wavefront compensation. This track loop has been accomplished conventionally by simple integral feedback control [1].

The purpose of this paper is to design a control system that optimally rejects disturbances in the sense of minimizing the variance of the error in the position of the laser beam. The two-input-two-output (two-axis) transfer function mapping mirror commands to the position of the beam image on the sensor is identified from experimental input-output data. This transfer function is converted to a balanced state-space plant model that is used in the control design for optimal disturbance rejection.

In the experiment, the performance of the optimal disturbance-rejecting controller is first compared to that of a standard LQG regulator. Both controllers were used to reject broadband disturbance with a 20 Hz bandwidth. In typical applications, atmospheric turbulence induces beam wandering with frequency content of up to 30 Hz [1,4]. Therefore, the optimal controller was retested for a disturbance bandwidth of 30 Hz. The latter test also demonstrates how well the optimal rejection controller performed when the actual disturbance spectrum varied from the disturbance spectrum for which the controller was designed.

The rest of this paper is divided into five sections. Section II describes the experimental setup. Section III describes the system identification procedure and results. Section IV describes a process for embedding a known disturbance into an augmented plant for the formulation of an optimal control and Kalman filtering problem. Section V presents experimental results and discusses their significance for the performance of the beam steering system. Section VI summarizes the results of the paper and suggests future research.

II. Experimental Setup

The main components of the beam steering experiment, shown in Figure 2.1, are a 635nm laser, two beam steering mirrors (BSM 1 and BSM 2), and a position sensing device that measures the position of the image that the laser beam forms on a fixed plane. The steering mirror labeled BSM 1 is used as the control actuator, while the mirror labeled BSM 2 is used to add disturbance to the beam. These two steering mirrors are controlled by independent PCs running under the real-time control program xPC target.

Manuscript submitted March 5, 2004. This work was supported by the U.S. Air Force Office of Scientific Research under Grant F49620-02-01-0319.

The authors are with the Mechanical and Aerospace Engineering Department, University of California, Los Angeles 90095-1597 (e-mail: pawel@ucla.edu, ttsao@seas.ucla.edu). Corresponding author: Steve Gibson (telephone: 310-825-9362, FAX: 310-206-2302, email: gibson@ucla.edu).

Each steering mirror is driven about X and Y axes by two piezo-electric actuators. Significant hysteresis associated with piezo-electric actuators presents a need for feedback control.

Tilting the mirrors about two orthogonal axes produces displacements of the laser image in corresponding X and Y directions in the sensor plane. These sensed X and Y image displacements are sampled and processed by the feedback control software running on the PC that drives the control actuator BSM 1. The sample-and-hold frequency for this system was chosen to be 1 KHz.

Figure 2.2 is a schematic of the proposed digital controller and how it interfaces with control mirror and position sensing device.

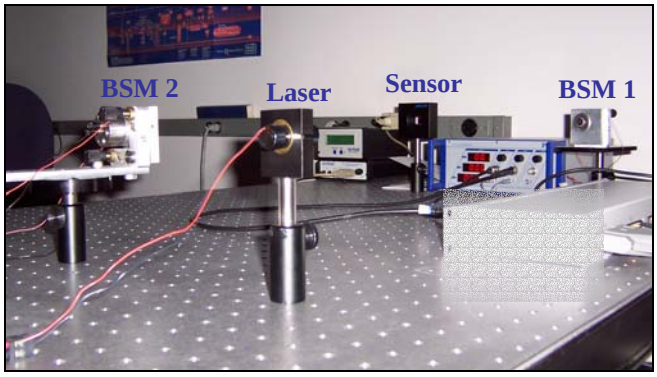

Fig. 2.1. Experimental Setup.

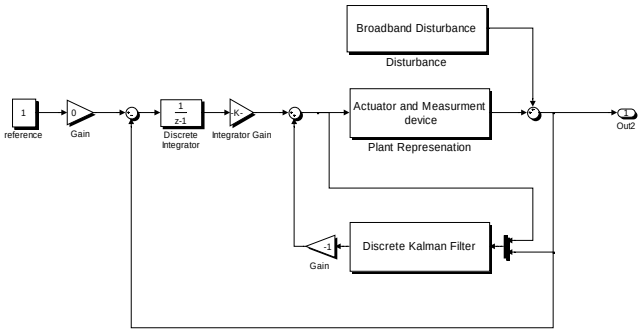

Fig 2.2. Each channel is represented as an independent SISO system.

III. System Identification and Verification

The cross-coupling between the two channels was the initial factor in control design. Based on the magnitude of coupling decision was made whether the two channels demand multi input multi output (MIMO) or two separate single input single output (SISO) control. To test for independence of the channels, a control sequence with 20Hz bandwidth was used to drive one of the actuators (either X or Y axis), and the both X and Y output channels were measured. When the X actuator was driven, the amplitude of X output was approximately 10 times the amplitude of the Y output, and vice versa. The authors concluded that the relatively small coupling between the two channels could be neglected for the research presented here, so that henceforth the X and Y channels are modeled as a pair of uncoupled SISO systems.

Because of the SISO assumption, the two channels were identified independently. The discrete-time transfer function of each channel is represented by the ARX (auto-regressive with exogenous input) model

$$y(k)+\sum_{i=1}^{N} A_i y(k-i)=\sum_{i=0}^{N} B_i u(k-i), \qquad (3.1)$$

which was identified by least-squares parameter estimation from experimental input/output data.

A designed broadband sequence with cut-off frequency of 50Hz was an input to the unidentified system. The cut-off frequency is a function of Nyquist frequency as its upper bound, in order to overcome difficulties due to aliasing, in this application cut-off frequency was first picked to be less than 500Hz. In addition due to environment disturbance such as, a 60Hz resonant frequency due to AC current, 120 Hz harmonics introduced by the artificial lighting and vendor's specs of the actuator's bandwidth (in this case how well can the actuator track the input) lead the author to believe a 50Hz frequency will be sufficient for this identification. Next for various N orders of the filter coefficients of the ARX model are extracted from (3.1) where y(k) is the output sequence, and u(k) is the input sequence. Observer-form state-space models were constructed from the ARX models, and balanced state-space realizations were then computed. The singular values associated with each balanced realization indicated the order for numerically well conditioned reduced-order plant model that captured the important input-output characteristics of the optical system. A large drop in the singular values of the balanced realization indicates that the states associated with the small singular values can be eliminated.

This analysis could be performed by comparing full-size and truncated systems' Bode plots, if the frequency response in frequency of interest is insignificant this suggests the truncated system is good enough and further truncation and analysis should be performed to get the smallest order transfer function. Another useful metric in choosing an appropriate system order is to compute measurement output errors in the identified system. This is accomplished in the following equation:

$$\frac{\left\| Modeled\_Output - True\_Measured\_Output \right\|_2}{\left\| True\_Measured\_Output \right\|_2} \quad (3.2)$$

Where the numerator is a 2 norm of difference between identified model output and a true measured output, and the denominator is the 2-norm of the true measured output. Furthermore to improve the analysis of the newly identified system authors of this paper suggest to filter the input sequence that was not used in the original ARX model identification, feed it through the identified system and then perform the analysis described in (3.2).

This system identification was performed with the data obtained from the experiment. Initially transfer function was assumed to be of order 8, and a 2-norm measure how good model approximation was computed to be 0.393360.

The singular values for the eight-order model implied that the order of the model should be reduced to 3 by balanced truncation. The bode plot of the third-order balanced realization is shown in Figure 3.1. For this third-order plant model, the 2-norm measure of model fit to data in (3.2) is 0.109449, almost four times better than previous result.

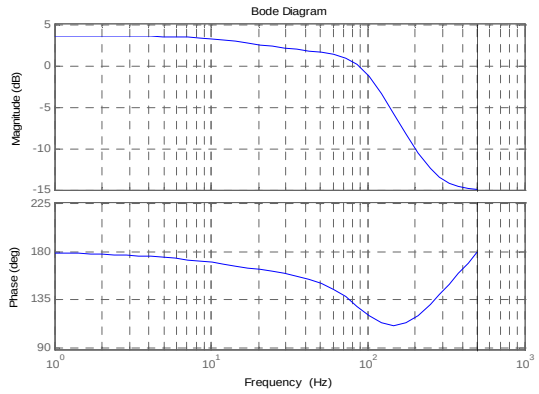

Fig 3.1 Identified plant with a 3rd order ARX model. Singular Values where calculated to be 0.7042, 0.1089, 0,0745;

The third-order realization was further truncated to a second-order realization, for which the noise contribution error calculated with (3.2) was 0.138347, obviously larger than 0.109449, value that was calculated with the third-order model. The same procedure was applied to the channel *Y* and likewise a third-order ARX model showed to be the best fit according to the criterion in (3.2).

In addition solely for purpose of demonstrating how well the identified model performs vs. the true measured outputs Figure 3.2 illustrates a tracking performance of the filter.

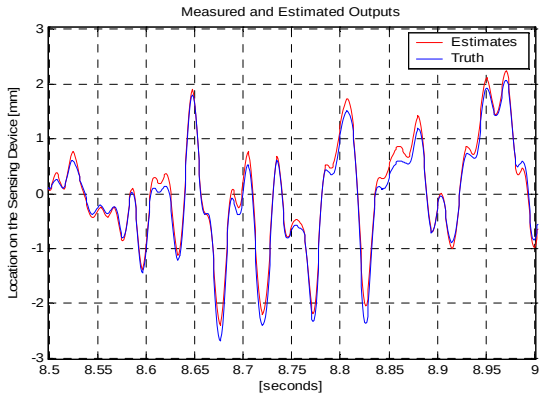

Fig 3.2 Comparison between measured output and estimated output in identified *X* channel

IV. Optimal Controller Design

A. Plant and disturbance models

The identified plant can be realized by the equations

$$\begin{aligned} x_p(k+1) &= A_p x_p(k) + B_w w_p(k) + B_u u(k) \\ y_p(k) &= C_p x_p(k) + \begin{bmatrix} 0 & d_{21p} \end{bmatrix} w_p(k) + d_{22p} u(k) \end{aligned} \quad (4.1)$$

where the vector $w_p(k)$ combines process and measurement noise effects due to the un-modeled disturbance such as actuator, sensor noise or the vibrations of the optical bench. To enable the controller to track low-frequency position commands and disturbances, an integrator is appended to the plant model for each of the *X* and *Y* channels. Each integrator has the form

$$x_i(k+1) = x_i(k) + r - y(k) \quad (4.2)$$

where *r* is the reference command and the integrator state is combined with the state vector x_p as in [5].

The disturbance added to the laser beam by the disturbance actuator BSM #2 is modeled as the output of a third-order Butterworth filter driven by a white-noise sequence $w_d(k)$. The bandwidth of the Butterworth filter is then the bandwidth of the modeled disturbance. For control design, the following state-space realization of Butterworth filter is used:

$$\begin{aligned} x_d(k+1) &= A_d x_d(k) + B_d w_d(k) \\ y_d(k) &= C_d x_d(k) \end{aligned} \quad (4.3)$$

For convenience in the control design, the direct feed-through term in the Butterworth filter was eliminated by adding delay to the filter and increasing the order of the disturbance model by one. This does not affect the statistics of the disturbance.

The expanded plant model includes the states of the identified beam steering system, the integrator, and the disturbance model defined by equations

$$x(k+1)=\begin{bmatrix} A_p & 0 & 0 \\ 0 & A_d & 0 \\ -C & -d_{21p}C_d & 1 \end{bmatrix}\begin{bmatrix} x_p(k) \\ x_d(k) \\ x_i(k) \end{bmatrix}+\begin{bmatrix} B_u & 0 & 0 \\ 0 & B_w & 0 \\ -d_{22p} & 0 & 1 \end{bmatrix}\begin{bmatrix} u(k) \\ w(k) \\ r(k) \end{bmatrix} \quad (4.4)$$

$$w(k)=\begin{bmatrix} w_p(k) \\ w_d(k) \end{bmatrix}$$

$$y(k)=\begin{bmatrix} C_p & d_{21p}C_d & 0 \end{bmatrix}\begin{bmatrix} x_p(k) \\ x_d(k) \\ x_i(k) \end{bmatrix}+d_{22p}u(k).$$

B. Minimum-variance beam control

In beam steering applications, the most important performance criterion for the optical system usually is the variance of the error in the image of the laser beam on a focal plane, like the plane of the position sensing device in the experiment described in this paper. Therefore, the appropriate optimal control problem here is to minimize the variance of the measured output y(k), and the optimal controller is an LQG controller for the expanded state-space model in (4.4).

For the control system with constant coefficients and the performance index:

$$J(x,u)=\sum_{k=0}^{\infty}\left(x^T(k)Qx(k)+u^T(k)Ru(k)\right) \quad (4.5)$$

The performance index is minimized by the state-feedback control law u(k)

$$u(k)=-K\begin{bmatrix} \hat{x}(k) \\ x_i(k) \end{bmatrix} \quad (4.6)$$

subject to state dynamics:

$$x(k+1)=\begin{bmatrix} A_p & 0 & 0 \\ 0 & A_d & 0 \\ -C & -d_{21p}C_d & 1 \end{bmatrix}\begin{bmatrix} x_p \\ x_d \\ x_i \end{bmatrix}+\begin{bmatrix} B_u \\ 0 \\ -d_{22p} \end{bmatrix}u(k) \quad (4.7)$$

where $\hat{x}(k)$ are the estimated states, output of the discrete time Kalman Filter. Since only plant and integrator are controllable by state-feedback, the state dynamic equation includes solely input characteristics associated with the direct input to the plant. The weighting matrix Q stated in (4.5) penalizes controllable states. In this experiment it takes on the following form

$$Q=\beta\begin{bmatrix} C_p \\ d_{21p}C_d \\ 1 \end{bmatrix}\begin{bmatrix} C_p & d_{21p}C_d & 1 \end{bmatrix} \quad (4.8)$$

where β is the tuning parameter.

The final step in this LQG control problem is to find the solution to the discrete Kalman filter problem. This involves finding the optimal gain matrix F. The new Q matrix punishes white noise sequences driving the plant and the disturbance models, it is formulated in equation

$$Q=B_wQ_wB_w^T. \quad (4.9)$$

The Q_w matrix was constructed with the use of relative weightings between white noise inputs driving the plant and white noise sequence driving the estimated disturbance model. Kalman filter's estimation performance of more heavily weighted states will improve at a cost of the states with less weighting. Equation below represents the system dynamics of the discrete time One-Step-Ahead Kalman Predictor.

$$x_k(k+1)=\begin{bmatrix} A_p & 0 \\ 0 & A_d \end{bmatrix}\begin{bmatrix} x_p(k) \\ x_d(k) \end{bmatrix}+\begin{bmatrix} \begin{bmatrix} B_u \\ 0 \end{bmatrix}[F] \end{bmatrix}\begin{bmatrix} u(k) \\ y(k) \end{bmatrix} \quad (4.10)$$

C. Simulation Results

Once all the components where calculated a closed loop form representation illustrated in the first section for each *X* and *Y* system were obtained. In order to observe how well the disturbance is rejected frequency response of the sensitivity function was plotted and compared against a sensitivity function obtained from a standard LQG problem. Next two figures, first illustrate the disturbance rejection by the means of a standard LQG regulator problem and the latter, the disturbance rejection transfer function obtained from the controller proposed in this paper. The disturbance model used in the experiment was a third-order Butterworth filter with cut-off frequency of 20Hz.

Simulation data in Fig 4.1 and Fig 4.2 clearly show a superior disturbance rejection in the 20Hz bandwidth, with only a slight amplification at higher frequencies when comparing against results obtained by standard LQG design. Results for the second SISO system controlling the *Y*-axis tilt were similar.

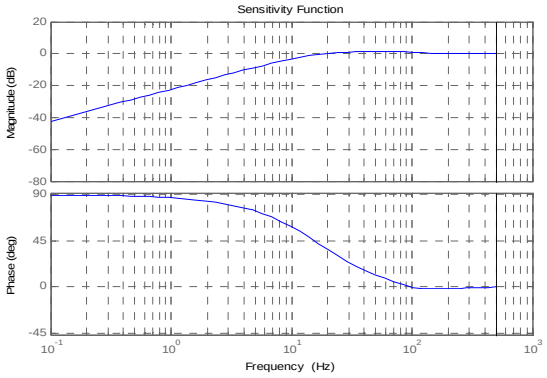

Fig 4.1 Sensitivity function for channel X controlled by LQG regulator with integral action.

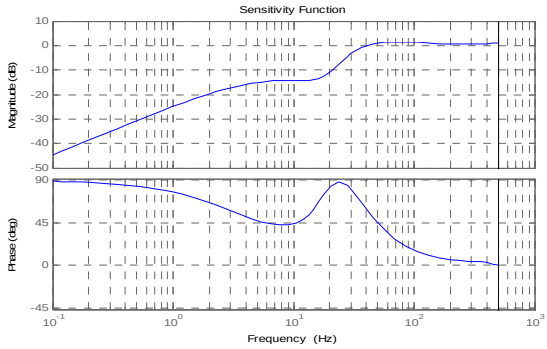

Fig 4.2 Sensitivity function for channel X controlled by proposed LQG regulator with integral and optimal disturbance rejection control.

V. EXPERIMENTAL RESULTS

This section presents the experimental results, and compares the performance of the optimal disturbance rejection controller to the performance of an LQG controller without the disturbance model.

Once the tuning LQG weighting matrices satisfied the design objectives, the actual gains and digital Kalman filter where downloaded to a CPU for real-time implementation. All experimental results ran for at least 10 seconds where 1000 data points per second were saved for further investigation. Since in many industry applications it is essential to keep the laser stabilized at a particular point, objective of this experiment was to simulate an auto-alignment problem meaning to keep the beam at the center of the position sensing device and reject any disturbance due to optical bench motion and disturbance from BSM2. The output measurements of the X and Y channels ideally should be (0,0). Figure 5.1 shows the measured X and Y output sequences from an experiment. Case I: open loop; Case II: standard LQG control; Case III: LQG control with optimal disturbance rejection. Comparison of these time data sequences confirms that the proposed controller significantly improves disturbance rejection.

Statistical values provide more analytical insight. Table V.1 shows the experimental values of the output-error variances in each of the three cases, along with the values predicted by simulation.

	Experiment	Simulation
Case I.	$\sigma_y^2 = 0.40903$ $\sigma_x^2 = 0.40253$	$\sigma_y^2 = 0.40903$ $\sigma_x^2 = 0.40253$
Case II.	$\sigma_y^2 = 0.15378$ $\sigma_x^2 = 0.16294$	$\sigma_y^2 = 0.19311$ $\sigma_x^2 = 0.18746$
Case III.	$\sigma_y^2 = 0.075085$ $\sigma_x^2 = 0.046533$	$\sigma_y^2 = 0.02114$ $\sigma_x^2 = 0.01941$

Table V.1 Experimental vs. Simulation results.

Since variance is a measure of performance throughout the entire frequency spectrum, another useful tool to examine is the power spectrum density of the measured outputs for the frequency range of interest. Inspecting the PSD plots proved once again that the controller in Case III operates much better at a lower frequency range due to its optimal disturbance rejection design. Additional implementation of integral control in both LQG designs also conjointly helps to cancel low frequencies.

Figure 5.1 depicts histogram data of twelve seconds of recorded measurements from channel X, similar results were observed for the channel Y. The X coordinates of these positioned measurements varied from -2.5 mm to +2.5 mm. This data was distributed among bins of 0.1 millimeter width. The number of data points is represented by the vertical axis in histograms. It is interesting to note that the performance of open loop as expected due to bias and drift terms was inadequate and did not satisfactorily stabilize the beam at the center of the sensing device. For the optimal feedback realization Case II, the beam was stabilized at the center of the sensing device, but once again it was outperformed by the controller realized in Case III.

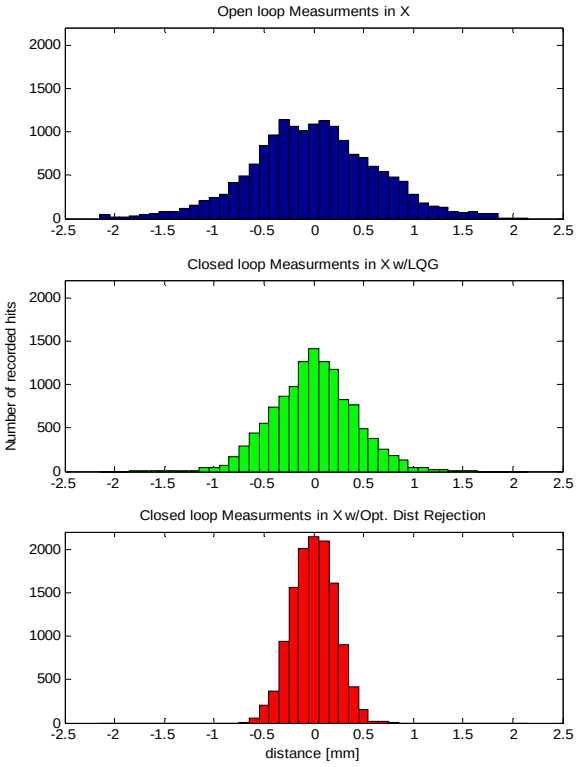

Fig 5.1 Graphs representing what measurements were recorded at what locations and how many times in an experiment that ran for approximately 12 seconds.

Finally, an experiment was conducted to test how the disturbance-rejecting controller performs when the actual disturbance bandwidth is different from the bandwidth of the disturbance model used in designing the controller. This is an important question, since it is impossible to know *a priori* the exact disturbance spectrum that the optical system will experience in practical applications.

The design of the disturbance-rejecting controller again assumed a 20Hz disturbance bandwidth. In the experiment, both the LQG controllers with and without the 20Hz disturbance model were used in the presence of a disturbance with 30Hz bandwidth. Statistical results, based on the collected output data are presented below in Table V.2.

Standard LQG Regulator	Proposed Controller
$\sigma_y^2 = 0.36620$	$\sigma_y^2 = 0.119040$
$\sigma_x^2 = 0.32979$	$\sigma_x^2 = 0.065191$

Table V.2 Experimental results with a 30Hz disturbance.

Improvement of factor of three is accomplished by the proposed controller. Furthermore Figure 5.2 illustrates the difference on the performance between the two controllers in low frequency spectrum. Controller designed with 20Hz optimal rejection, still outperforms the standard LQG even if the actual disturbance used was 30Hz. Naturally excellent rejection in the low frequencies comes at a price of amplifying response of higher frequency components, but since the amplification occurs well below -30dB it does not pose a significant problem.

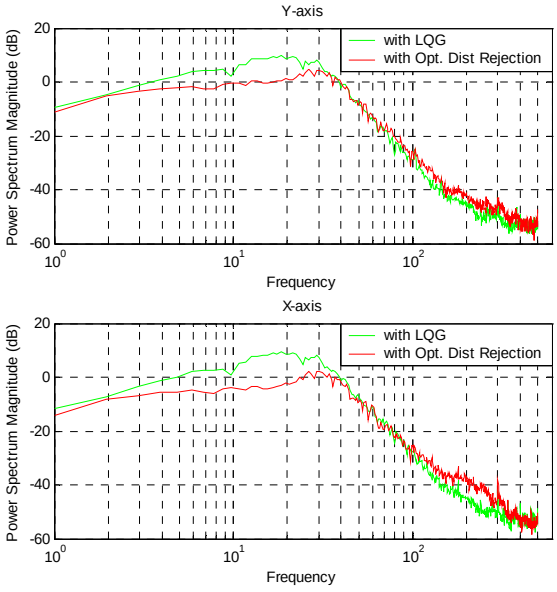

Fig 5.2 Power spectral densities of measured outputs in two different controller implementations.

VI. Conclusions

The design and analysis with emphasis on optical and laser beam control applications of the LQG regulator controller with optimal disturbance rejection was described in this paper. The design process including a strategic weighting of matrices to minimize the performance index was extensively used in the solution of this problem. Several guidelines on how to vary the design based on sensitivity plots and closed loop response Bode plots were also discussed.

The experimental result in section V verified the design predictions and demonstrated that the controller performed exceptionally well. The variance of the minimized error was more than five times less once compared to open loop measurements and almost three times less when compared to a standard LQG regulator with integral action. The controller also outperformed a standard LQG regulator in a simulated beam wandering disturbance environment which was different from that used for its design.

Finally, to compensate for the weather dependent changing disturbance characteristics, adaptive outer loop [4,5] can be added to the LQG control presented in this paper to provide consistent optimal performance.

References

[1] Robert K. Tyson, "Introduction to Adaptive Optics, SPIE Press, Bellingham, WA. 2000.

[2] J. S. Gibson, C.-C. Chang, and B. L. Ellerbroek, "Adaptive optics: wavefront correction by use of adaptive filtering and control," Applied Optics, Optical Technology and Biomedical Optics, vol. 39, no. 16, pp. 2525–2538, June 2000.

[3] B.-S. Kim, J. S. Gibson, and T.-C. Tsao, "Adaptive Control of a Tilt Mirror for Laser Beam Steering," *American Control Conference*, Boston, MA, June 2004.

[4] James R. Dunphy, and J. Richard Jerr, "Turbulence effects on target illumination by laser sources: phenomelogical analysis and experimental results," Applied Optics, Vol 16, No. 5, pp. 1345-1358, May 1977.

[5] Gene F. Franklin, J. David Powell, Abbas Emami-Naeini, "Feedback Control of Dynamic Systems (Book Style) *Plastics*, 4th ed. Upper Saddle River, New Jersey : Prentice Hall, 2002, pp. 587–588.